The fibroblast-derived protein PI16 controls neuropathic pain

Pooja Singhmar[a], Ronnie The Phong Trinh[a], Jiacheng Ma[a], XiaoJiao Huo[a], Bo Peng[b], Cobi J. Heijnen[a], and Annemieke Kavelaars[a,1]

[a]Laboratories of Neuroimmunology, Department of Symptom Research, The University of Texas MD Anderson Cancer Center, Houston, TX 77030; and [b]Department of Bioinformatics & Computational Biology, The University of Texas MD Anderson Cancer Center, Houston, TX 77030

Edited by Tomas G. M. Hökfelt, Karolinska Institutet, Stockholm, Sweden, and approved January 29, 2020 (received for review August 4, 2019)

Chronic pain is a major clinical problem of which the mechanisms are incompletely understood. Here, we describe the concept that PI16, a protein of unknown function mainly produced by fibroblasts, controls neuropathic pain. The spared nerve injury (SNI) model of neuropathic pain increases PI16 protein levels in fibroblasts in dorsal root ganglia (DRG) meninges and in the epi/perineurium of the sciatic nerve. We did not detect PI16 expression in neurons or glia in spinal cord, DRG, and nerve. Mice deficient in PI16 are protected against neuropathic pain. In vitro, PI16 promotes transendothelial leukocyte migration. In vivo, *Pi16*$^{-/-}$ mice show reduced endothelial barrier permeability, lower leukocyte infiltration and reduced activation of the endothelial barrier regulator MLCK, and reduced phosphorylation of its substrate MLC2 in response to SNI. In summary, our findings support a model in which PI16 promotes neuropathic pain by mediating a cross-talk between fibroblasts and the endothelial barrier leading to barrier opening, cellular influx, and increased pain. Its key role in neuropathic pain and its limited cellular and tissue distribution makes PI16 an attractive target for pain management.

Peptidase inhibitor 16 | PI16 | neuropathic pain | perineurium | fibroblasts

More than one-third of the United States population and ~1.5 billion people worldwide face chronic pain (1). In the United States, the costs of chronic pain are an estimated 30% higher than the combined costs of cancer, heart disorders, and diabetes (2). Treatment of chronic pain is still a major challenge and especially in view of the opioid crisis, better understanding of the cellular and molecular mechanisms underlying chronic pain is urgently needed.

We showed previously that mice deficient in G protein coupled receptor kinase 2 (GRK2) develop persistent pain in multiple models (3–6). In this study, in a serendipitous discovery based on RNA sequencing (RNA-seq) analysis of dorsal root ganglion gene expression comparing GRK-deficient and wild-type (WT) mice, we identified peptidase inhibitor 16 (PI16) as a potential regulator of persistent pain. PI16 is a poorly characterized member of the CAP (Cysteine-rich secretory proteins, Antigen 5, and Pathogenesis-related 1) superfamily of proteins that is highly conserved across species. PI16 is predicted in the Conserved Domain Database (https://www.ncbi.nlm.nih.gov/cdd) to have an extracellular role and to possess protease enzymatic activity (7). Very little is known about the tissue distribution and function of PI16. What is known is that PI16 is expressed in cardiac fibroblasts, but PI16-deficient mice do not have a cardiac phenotype (8, 9). There is evidence that PI16 regulates processing of the chemokine chemerin (9), cutaneous cathepsin K (10), and the matrix metalloprotease MMP2 (11). There is no previous evidence for a role of PI16 in pain signaling. Here, we demonstrate that PI16 plays a key role in chronic pain and is expressed in fibroblasts in the meninges of the dorsal root ganglia (DRG) and the perineurium, but not by neurons or glia.

Results

Identification of Pi16 as a Gene Associated with Pain. To identify regulators of chronic pain, we compared gene expression profiles between DRG from female WT and *Grk2*$^{+/-}$ mice at 5 h after intraplantar PGE_2. We selected this model because we showed earlier that female WT mice recover within hours from PGE_2-induced allodynia, whereas *Grk2*$^{+/-}$ mice show allodynia for at least 3 wk (3–5).

Only five differentially expressed genes (*Pi16*, *Gm12250*, *Iigp1*, *Gbp2*, *Irgm2*) were identified (Fig. 1*A* and *SI Appendix*, Fig. S1*A*) after elimination of genes that differed by genotype in the absence of PGE_2 (*SI Appendix*, Fig. S2). Of these five genes, we further pursued *Pi16* because it is a gene with unknown function in pain and is highly conserved in eukaryotes, including a high degree of homology between mouse and human PI16. Pi16 mRNA expression was decreased in DRG from female WT mice during recovery from PGE_2 allodynia but did not change in DRG from female *Grk2*$^{+/-}$ mice who developed persistent allodynia (Fig. 1*B*). Time course analysis in a separate group of male WT mice confirmed that Pi16 mRNA levels decrease during resolution of PGE_2-induced allodynia and return to baseline levels at 48 h after PGE_2 (*SI Appendix*, Fig. S1*B*).

Pi16 Knockout Mice Are Protected Against SNI-Induced Pain. Using the spared nerve injury (SNI) model of chronic neuropathic pain, we show that male and female *Pi16*$^{-/-}$ mice were protected against mechanical allodynia (Fig. 1*C*). Mechanical sensitivity at

Significance

Chronic pain is a major clinical problem and treatments are only partially effective and/or have addiction liability. Therefore, we need novel treatments. We identified a regulator of pain: the protease inhibitor PI16. Mice deficient in Pi16 are protected against neuropathic pain. Interestingly, PI16 is not made by neurons, glia, or immune cells but is mainly produced by fibroblasts surrounding the peripheral and central nervous system. Mechanistic studies indicate that PI16 promotes pain by increasing the permeability of the blood nerve barrier leading to increased immune cell infiltration. In summary, PI16 plays a key role in pain and has a limited cellular and tissue distribution, making PI16 an attractive target for pain management.

Author contributions: P.S., C.J.H., and A.K. designed research; P.S., R.T.P.T., J.M., and X.H. performed research; P.S., B.P., C.J.H., and A.K. analyzed data; and P.S., C.J.H., and A.K. wrote the paper.

The authors declare no competing interest.

This article is a PNAS Direct Submission.

Data deposition: RNA-sequencing data reported in this paper have been deposited in Zenodo repository (https://zenodo.org/record/3473295).

[1]To whom correspondence may be addressed. Email: akavelaars@mdanderson.org.

This article contains supporting information online at https://www.pnas.org/lookup/suppl/doi:10.1073/pnas.1913444117/-/DCSupplemental.

First published February 20, 2020.

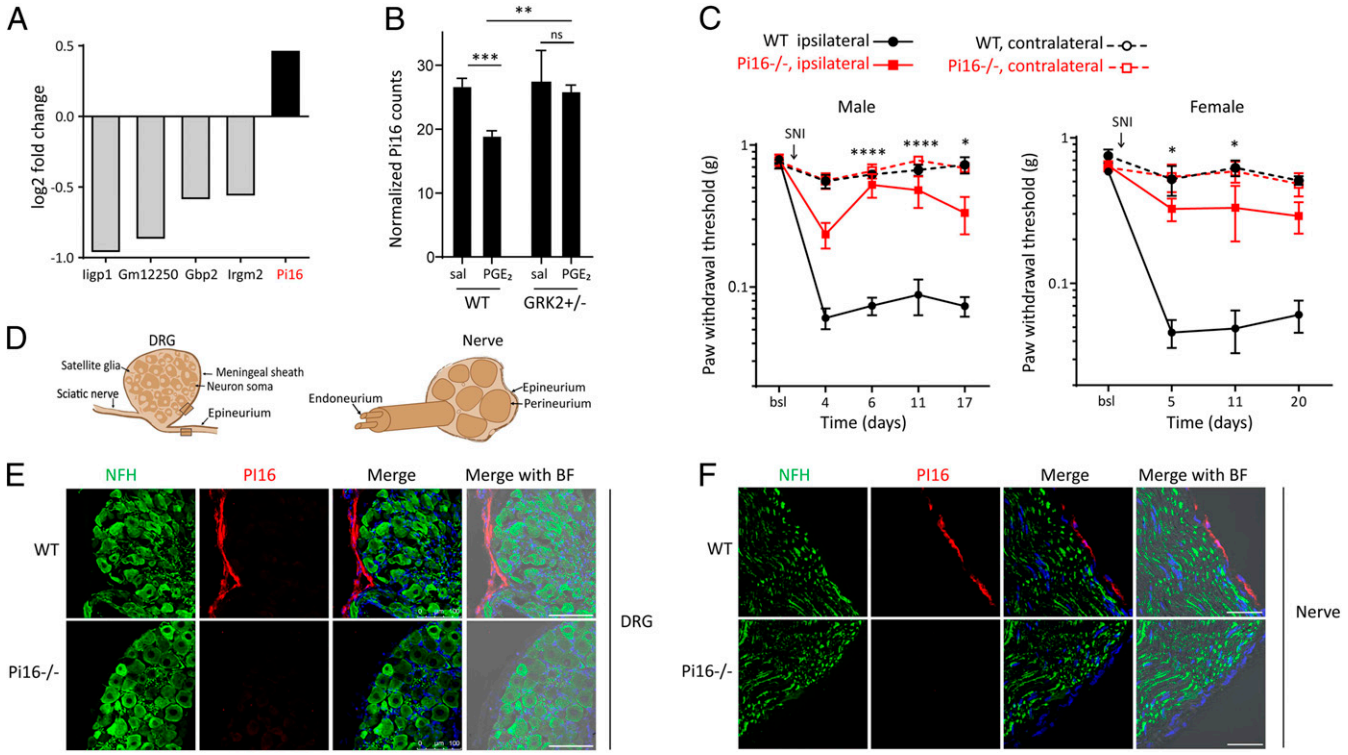

Fig. 1. Identification of Pi16 as a gene associated with pain and PI16 is localized in the meninges of DRG and the epi/perineurium. (*A*) Differentially expressed genes as identified by RNA-seq analysis of lumbar DRGs from female WT ($n = 3$) and *Grk2*$^{+/-}$ ($n = 3$) mice collected 5 h after PGE2 treatment (100 ng per paw). Fold change is based on counts per million reads adjusted for multiple testing error (false discovery rate < 0.05) (also see *SI Appendix*, Fig. S1). (*B*) Expression of Pi16 mRNA in lumbar DRGs of saline (sal) and PGE2-treated female WT ($n = 3$) and *Grk2*$^{+/-}$ ($n = 3$) mice 5 h after PGE2 treatment as assessed by RNA-seq analysis. Data represent normalized log counts per million reads. ***$P < 0.001$; **$P < 0.01$; ns, not significant; two-way ANOVA followed by Bonferroni analysis. (*C*) SNI was performed on male WT ($n = 6$) and *Pi16*$^{-/-}$ ($n = 4$), and, female WT ($n = 4$) and *Pi16*$^{-/-}$ ($n = 5$) mice and mechanical allodynia was assessed using von Frey hairs in ipsilateral and contralateral hind paw at baseline (bsl) and over time after SNI. Two-way repeated-measures ANOVA: Male mice-time: $P < 0.0001$; genotype: $P < 0.001$; interaction: $P < 0.001$. Female mice-time: $P < 0.0001$; genotype: $P < 0.001$; interaction: $P < 0.045$. Post hoc Bonferroni analysis: *$P < 0.05$, ****$P < 0.0001$ for *Pi16*$^{-/-}$ vs. WT ipsilateral. (*D*) Schematic of DRG and sciatic nerve containing neuronal soma, glia, and blood vessels. The DRG is enclosed by a meningeal sheath. The epineurium surrounds the entire nerve and is present between the nerve fascicles. The perineurium surrounds the fascicles and the endoneurium surrounds the axons. Shaded box represents region where images were captured. (*E*) Representative lumbar DRG section from naïve WT and *Pi16*$^{-/-}$ mice stained for the neuronal marker NFH and PI16. (*F*) Representative sciatic nerve sections from WT and *Pi16*$^{-/-}$ mice stained for NFH and PI16. Right-most in *E* and *F*: Bright field (BF) image merged with green (NFH), red (PI16), and DAPI (blue). Images in *E* and *F* are representative of $n = 4$ mice per group, and additional examples are shown in *SI Appendix*, Fig. S4. (Scale bar, 100 μm.)

baseline and in the contralateral paw was not affected by genotype (Fig. 1*C*).

Protection of *Pi16*$^{-/-}$ mice against neuropathic pain was not due to changes in the distribution of DRG neurons or spinal cord dorsal horn neuron staining for NF200, CGRP, or IB4; in morphology and structure of myelinated and unmyelinated fibers in the sciatic nerve; or in the density of PGP^{+} intraepidermal nerve fibers (*SI Appendix*, Fig. S3).

PI16 Is Detected in Fibroblasts in the Meninges of the DRG and the Epi/Perineurium. Immunofluorescence analysis shows that under baseline conditions, PI16 protein is expressed in the meningeal sheath surrounding the DRG and in the epi/perineurium of the sciatic nerve, which is continuous with the meninges and surrounds the nerve fascicles and endoneurial space (12, 13) (Fig. 1 *D*–*F* and *SI Appendix*, Fig. S4 *A* and *B*). PI16 is not detectable in neurons or glia in the DRG or nerve (Fig. 1 *E* and *F* and *SI Appendix*, Fig. S4 *A* and *B*).

At the cellular level, PI16 is present in elongated cells with flat and wavy nuclei indicative of fibroblasts. Double staining for PI16 and the fibroblast markers α-SMA (alpha smooth muscle actin) or P4HB (collagen Prolyl 4-hydroxylase) confirmed expression of PI16 in fibroblasts (Fig. 2*A* and *SI Appendix*, Fig. S5). We did not detect any PI16 staining in GLUT-1–positive cells in the inner layer of the perineurium (Fig. 2*B*). Endothelial cells can express PI16 (11), but we did not detect PI16 in CD31- or CLDN1-positive endothelial cells in the DRG (Fig. 2*C*). However, PI16-positive fibroblasts were closely associated with endothelial cells (Fig. 2 *C*, *Top*). Whole-mount DRG staining also identified PI16-positive fibroblasts around the CD31^{+} vascular network (Fig. 2 *C*, *Middle*). PI16 is also expressed in fibroblasts in the meninges of the spinal cord (*SI Appendix*, Fig. S6), but not in spinal cord neurons or glia. PI16 was not detected in fibroblasts surrounding the central canal (*SI Appendix*, Fig. S6*C*).

PI16 Protein Levels in DRG and Sciatic Nerve Are Increased in Models of Neuropathic Pain. PI16 is mainly expressed as a 108-kDa protein in murine DRG, nerve (Fig. 3*A*), and in meninges of brain and spinal cord (*SI Appendix*, Fig. S6*D*). PI16 mRNA and protein are also expressed in human DRG samples, confirming that expression of PI16 in DRG is conserved between mouse and human (Fig. 3*B*).

SNI significantly increased PI16 protein levels in the ipsilateral compared to contralateral sciatic nerve and DRG as assessed at day 8 and day 22 (Fig. 3 *C* and *D*). Sham surgery did not affect PI16 levels (Fig. 3*C* and *SI Appendix*, Fig. S6*E*).

Immunofluorescence analysis showed that in the nerve and DRG, SNI induced an expansion of PI16-positive fibroblasts and

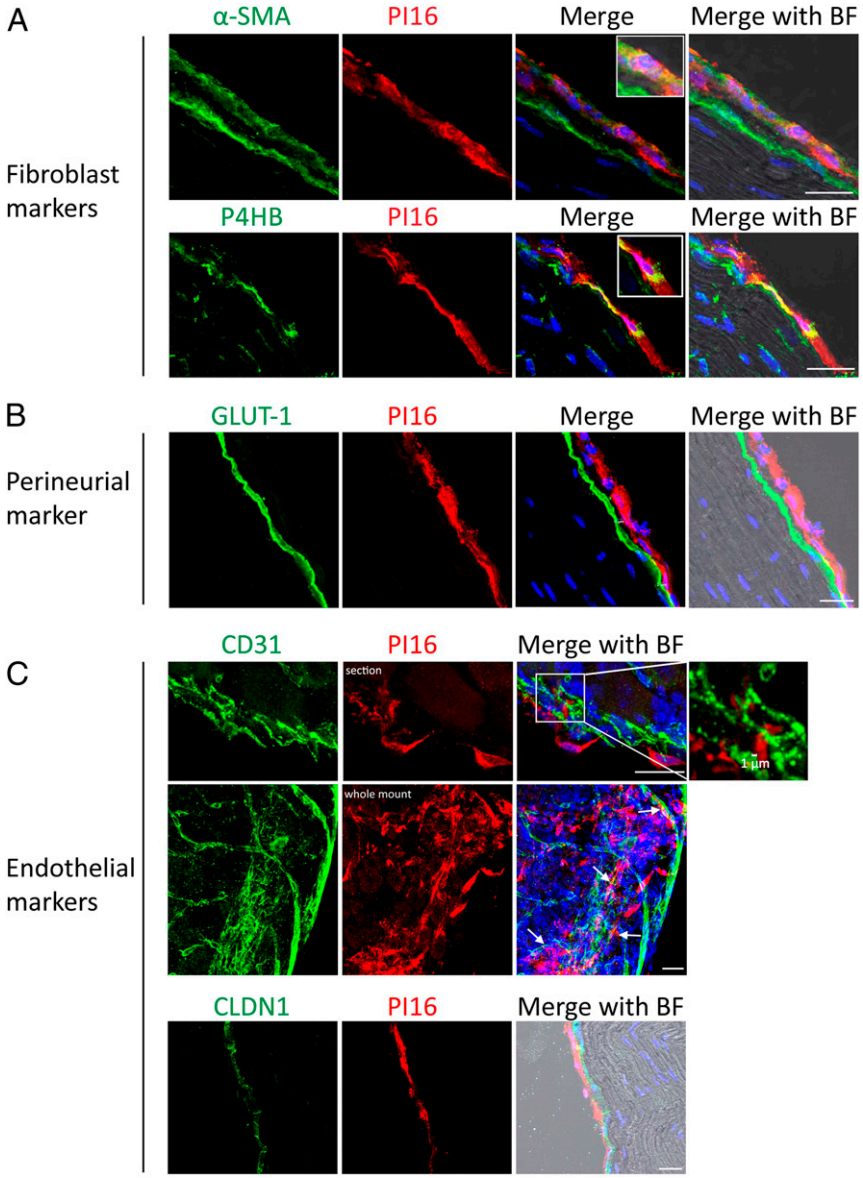

Fig. 2. PI16 is detected in fibroblasts in the meninges of the DRG and the epi/perineurium. Representative sciatic nerve section from naïve WT mice showing immunostaining of PI16 (red) with fibroblast markers α-SMA and P4HB (*A*), perineurial marker GLUT-1 (*B*), endothelial markers CD31 and CLDN1 (*C*). (*Top*) PI16-positive fibroblasts and endothelial cells are within 1 μm distance (indicated by arrows). (*Middle*) Staining of whole-mount DRG. Bright field (BF) image merged with other channels is shown. (Scale bar, 25 μm.) Images are representative of $n = 4$ for *A* and $n = 3$ for *B* and *C* mice per group. Additional examples are shown in *SI Appendix*, Fig. S5.

an increase in meningeal and epi/perineurial thickness on the SNI-ipsilateral side (Fig. 4 *A*–*E* and *SI Appendix*, Fig. S7). SNI-induced fibroblasts were predominantly positive for α-SMA and P4HB and coexpressed PI16 (Fig. 4 *A* and *C*). Sham surgery did not affect PI16 levels and epi/perineurial thickness when compared to SNI (Fig. 4 *A* and *B*). An expansion of PI16-positive fibroblasts was also observed around the injury site in the nerve (*SI Appendix*, Fig. S8). SNI did not induce detectable PI16 in neurons or glia in the DRG or nerve (Fig. 4 *A* and *D*).

After SNI, immune cells infiltrate into the DRG and nerve and expression of PI16 by a subset of memory T regulatory cells has been reported (14). However, SNI did not induce Pi16 in CD45-positive leukocytes in DRG or at the site of nerve injury (*SI Appendix*, Fig. S8*B*). PI16 was also not induced in chondroitin sulfate proteoglycan (NG2)-positive endoneurial fibroblasts, pericytes, and vasculature associated muscle cells (15, 16) (*SI Appendix*, Fig. S8*C*). SNI did not induce detectable changes in PI16 staining in the meninges of the spinal cord or in the dorsal horn of the spinal cord (*SI Appendix*, Fig. S6 *F* and *G*).

PI16 Is Secreted In Vitro by Perineurial Myofibroblasts. The SNI-induced increase in PI16 was mainly detected in α-SMA–positive fibroblasts. In vitro, differentiation of primary perineurial fibroblast into α-SMA–positive myofibroblasts using TGFβ1 increased PI16 protein levels in these cells and in the culture supernatant (Fig. 5 *A* and *B*), indicating PI16 is a secreted protein. As expected for a secretory protein, GFP-tagged PI16 overexpressed in fibroblasts localized to the endoplasmic reticulum and secretory vesicles (Fig. 5*C*).

Pi16 Deficiency Reduces the SNI-Induced Infiltration of Leukocyte into the DRG and Nerve. To get insight into the pathways via which Pi16 deficency protects against SNI-induced pain, we compared

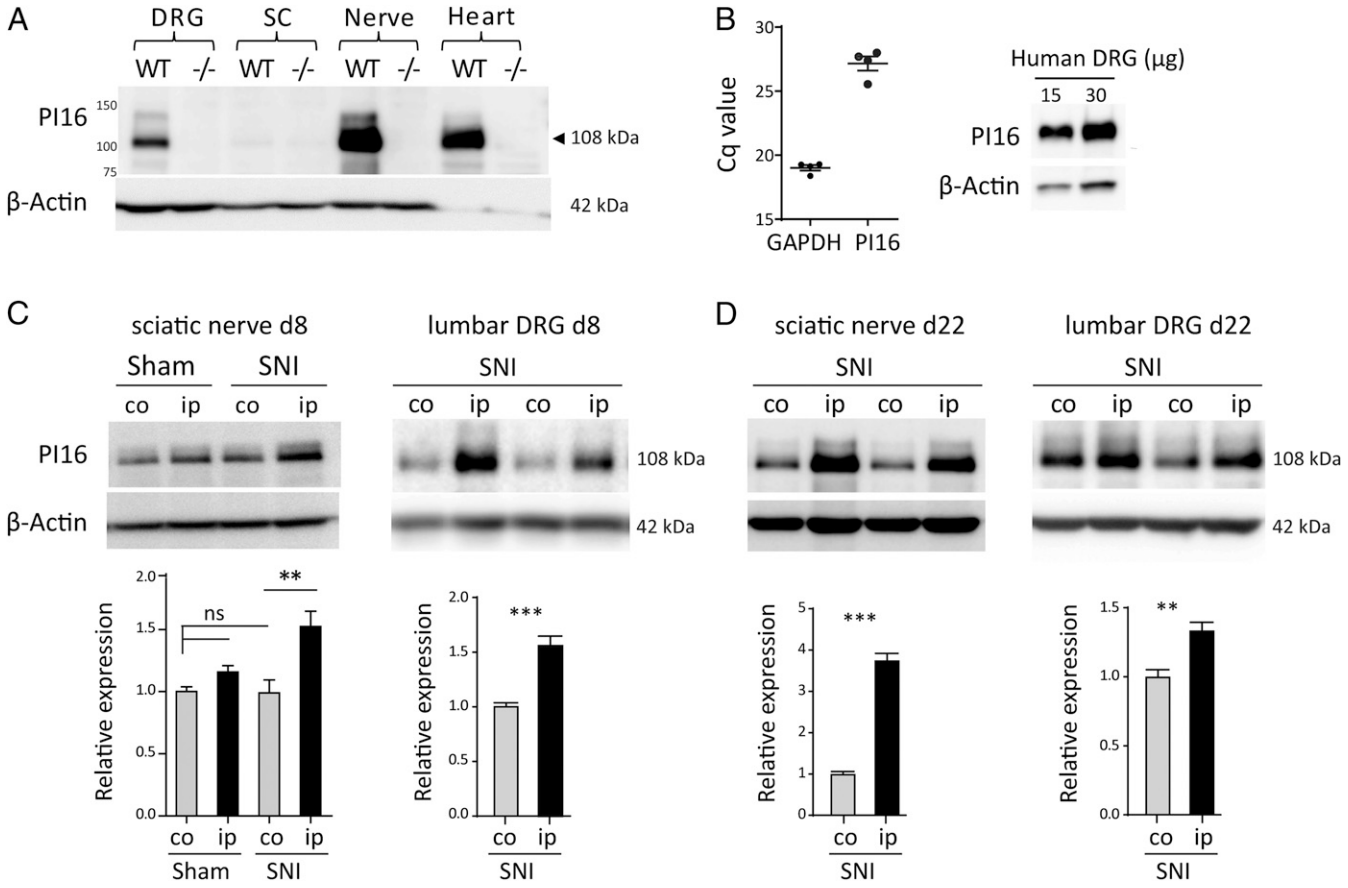

Fig. 3. SNI up-regulates PI16 protein levels in DRG and sciatic nerve. (*A*) Western blot analysis of PI16 in DRG, spinal cord, nerve, and heart tissue from male WT and *Pi16*$^{-/-}$ mice. PI16 is mainly expressed as a 108-kDa protein that is not present in samples from *Pi16*$^{-/-}$ mice confirming antibody specificity. (*B*, *Left*) qRT-PCR analysis of PI16 mRNA in three human DRG samples normalized for GAPDH. (*B*, *Right*) Western blot analysis of PI16 protein in a human DRG. (*C*) Western blot analysis of PI16 protein expression in contralateral (co) and ipsilateral (ip) sciatic nerve (from male mice) and lumbar DRG (from female mice) at 8 d after SNI or sham surgery. For DRG, representative blot shows PI16 expression in two animals per group. Bar graphs represent means ± SEM of n = 4 mice per group for sciatic nerve (ANOVA test, $^{**}P < 0.01$; ns, not significant) and $n = 6$ mice per group for DRG (Student's *t* test, $^{***}P < 0.001$). (*D*) Western blot analysis of PI16 protein expression in sciatic nerve and lumbar DRG at 22 d (from $n = 6$ male mice per group) after SNI surgery (Student's *t* test, $^{***}P < 0.001$, $^{**}P < 0.01$).

SNI-induced changes in the transcriptome of lumbar DRGs from WT and *Pi16*$^{-/-}$ mice by RNA-seq. SNI changed the expression of 4,074 genes in the DRG in WT mice and only 1,138 genes in *Pi16*$^{-/-}$ mice ($-2.00 < \log_2$ fold change < 2.00). In line with previous studies (17), Ingenuity Pathway Analysis (IPA) identified activation of canonical pathways associated with neurotransmission and inflammation, including "neuroinflammation signaling," "cAMP signaling," and "complement system" in response to SNI (*SI Appendix*, Fig. S9). Pathway activation scores were lower in *Pi16*$^{-/-}$ than in WT mice (*SI Appendix*, Fig. S9). Moreover, the pathways neuropathic pain signaling in dorsal horn and PKA signaling pathway were inhibited in *Pi16*$^{-/-}$ mice, while they were activated in WT mice. The top 20 up-regulated genes after SNI included pain-related genes like *Gpr151*, *Atf3*, *Gal*, *Cckbr*, *Nts*, and *Sema6a* in both WT and *Pi16*$^{-/-}$ mice with reduced expression in *Pi16*$^{-/-}$ compared to WT. TGFβ was among the most prominent upstream regulators driving changes in gene expression. Overall proinflammatory cytokine gene expression was reduced in lumbar DRG of *Pi16*$^{-/-}$ animals post-SNI as compared to WT-SNI (*SI Appendix*, Fig. S10).

Importantly, IPA disease and functions comparison analysis identified genotype differences in activation of immune cell migration and cell movement pathways, including leukocyte migration, inflammatory response, and quantity of cells (Fig. 6*A*). The genes driving these differences included macrophage (*Itgam*, *Csf1r*, *Ccl9*) and B/T cell (*Tnfrsf8*/CD30, CD72) markers.

Consistently, immunofluorescence analysis showed that after SNI, *Pi16*$^{-/-}$ mice had lower numbers of CD45-positive cells in the lumbar DRG (Fig. 6*B*) and nerve (*SI Appendix*, Fig. S11) than WT mice. The majority of these leukocytes stained positive for macrophage marker F4/80 (Fig. 6*B*).

Previous studies have identified two possible targets of PI16 that could contribute to changes in leukocyte migration/infiltration, i.e., the chemoattractant chemerin via inhibition of proteolytic activation and MMP2 via modification of its enzymatic activity (9, 11). However, we did not detect any difference in the expression of precursor and activated chemerin in the lumbar DRGs or in MMP2 activity as assessed by zymography between WT and *Pi16*$^{-/-}$ post-SNI (Fig. 6 *C* and *D*).

To identify a potential effect of PI16 on cell migration, we tested the transendothelial migration of monocytes in the presence of PI16-conditioned medium in vitro. Monocytes were allowed to migrate across a monolayer of TNF-α–treated endothelial cells in response to CXCL12. CXCL12 is a potent chemoattractant that was increased in the DRG in response to SNI in our RNA-seq data. PI16 conditioned medium increased monocyte migration across the endothelial barrier (Fig. 6*E*). PI16-conditioned medium did not affect migration in the absence of the endothelial barrier or in the absence of CXCL12.

Opening of the endothelial barrier is a crucial step allowing influx of leukocytes into the injured tissue. Our RNA-seq data revealed lower levels of nonmuscle Mylk, a well-established

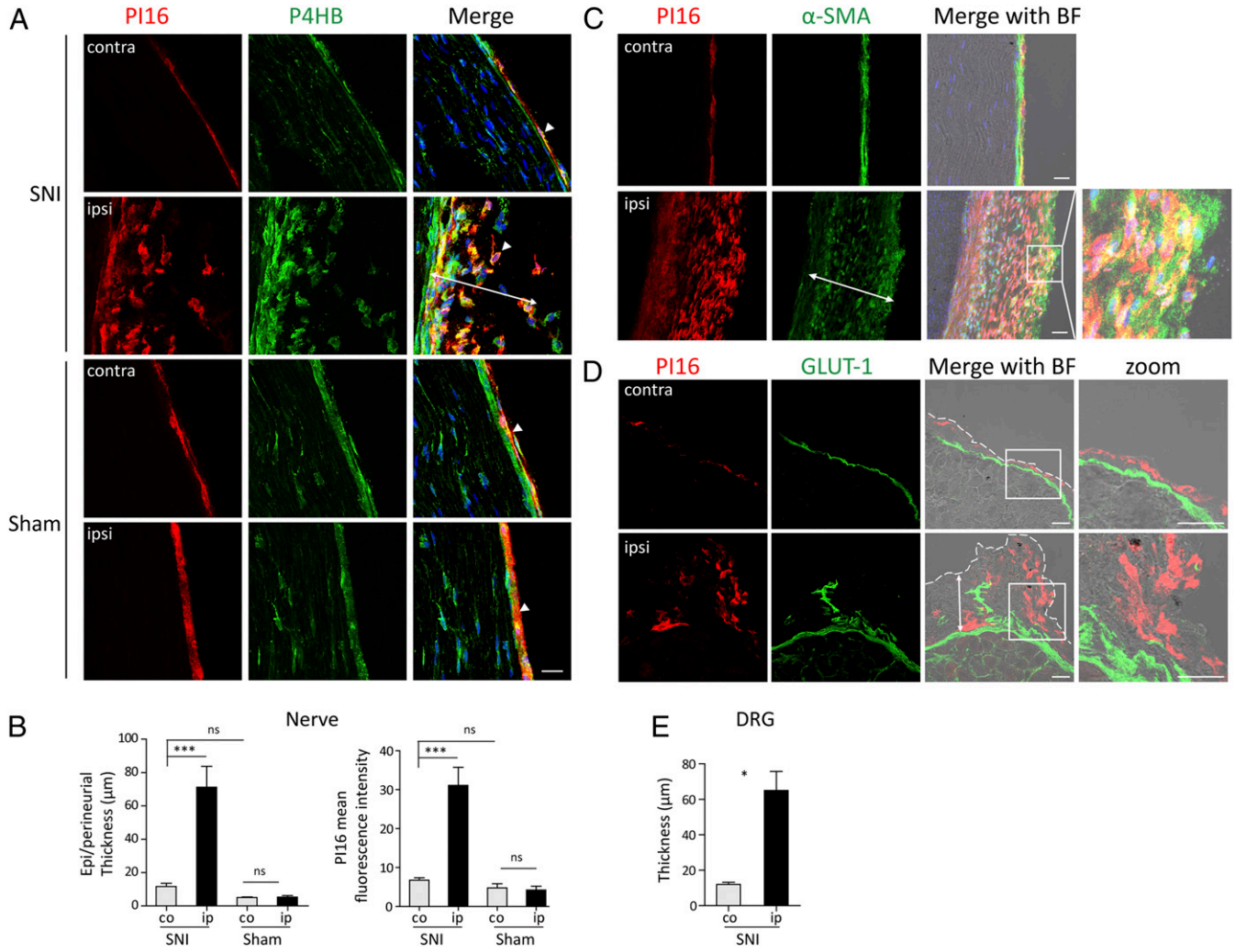

Fig. 4. SNI-induced increase in fibroblast Pi16 levels. (*A*) Representative images showing PI16 (red) and P4HB (green) staining in contralateral (contra) and ipsilateral (ipsi) sciatic nerve after SNI and sham surgery. Note PI16 in P4HB-positive fibroblasts (arrowheads). Note expansion of P4HB positive fibroblasts in the epi/perineurium coexpressing PI16 specifically in the SNI-ipsilateral nerve. (*B*) Quantitation of epi/perineurium thickness (double headed arrows in *A* and *C*) and PI16 mean intensity in contralateral (co) and ipsilateral (ip) side after Sham and SNI surgery is shown. One way-ANOVA test: ***$P < 0.001$; ns, not significant. $n = 4$–9 male mice per group. (*C*) Representative image showing PI16 (red) in α-SMA (green) positive fibroblast in sciatic nerve after SNI. Note expansion of α-SMA–positive fibroblasts coexpressing PI16 in the ipsilateral nerve. BF (bright field) image merged with PI16, α-SMA, and DAPI (blue) is shown. (*D*) Representative image of PI16 (red) and GLUT-1 (green) staining in lumbar DRG contralateral (contra) and ipsilateral (ipsi) to SNI surgery. BF image merged with PI16 and GLUT-1 is shown. The zoom images show a magnified view of the area outlined by the square. Perineurial GLUT-1 (green) staining marks the border of DRG, and the dotted white line marks the edge of the meningeal sheath. Note the PI16 staining in the meningeal sheath and increased PI16 outside GLUT-1 (double headed arrow) in the meninges of ipsilateral DRGs. (*E*) Quantitation of meningeal thickness (double headed arrows in *D*) in lumbar DRG after SNI. Meningeal sheath outside GLUT-1 (which labels inner layer of the perineurium) was measured. *t* test: *$P < 0.05$. Immunofluorescence data are representative of $n = 3$ mice for contralateral and $n = 5$ for ipsilateral. (Scale bar, 25 μm.)

regulator of the endothelial barrier, in DRGs from *Pi16*$^{-/-}$ mice post-SNI (Fig. 6*F*). Mylk encodes myosin light chain kinase (MLCK) and MLCK-mediated phosphorylation of myosin light chain-2 (MLC-2) promotes endothelial barrier permeability (18). Notably, experiments in a separate group of mice showed that *Pi16*$^{-/-}$ mice were protected against the SNI-induced increase in pMLC2 in ipsilateral DRGs and sciatic nerve (Fig. 6 *G* and *I*). MLC-2 is expressed by CD31-positive endothelial cells in close proximity to PI16 containing fibroblasts (Fig. 6*H*).

To determine whether the reduced levels of pMLC2 in *Pi16*$^{-/-}$ mice were associated with reduced endothelial permeability after SNI, we injected the fluorescent tracer sodium fluorescein (NaFlu) intravenously. NaFlu accumulation was significantly lower in sciatic nerve of *Pi16*$^{-/-}$ mice than in WT mice (Fig. 6*J*), indicating that PI16 contributes to the SNI-induced increase in endothelial barrier permeability.

Discussion

Our findings provide evidence for a key role of the putative protease inhibitor PI16 in pain. We show that *Pi16*$^{-/-}$ mice are protected against mechanical allodynia in the SNI model of chronic neuropathic pain. We show that SNI increases expression of PI16 in DRG and sciatic nerve. Notably, at baseline or after SNI, PI16 is not detectable in neurons, glia, leukocytes, or endothelial cells, but only in meningeal and epi/perineurial fibroblasts. In vitro, PI16 enhances transendothelial migration of monocytes. In vivo, *Pi16*$^{-/-}$ mice are protected against the SNI-induced increase in endothelial permeability and against the increase in leukocyte infiltration into the DRG and nerve. We propose that PI16 secretion by fibroblasts in DRG meninges and epi/perineurium represents a crucial permissive signal for establishment of chronic pain through promoting vascular permeability and leukocyte infiltration via a pathway involving increased MLCK-dependent phosphorylation of the

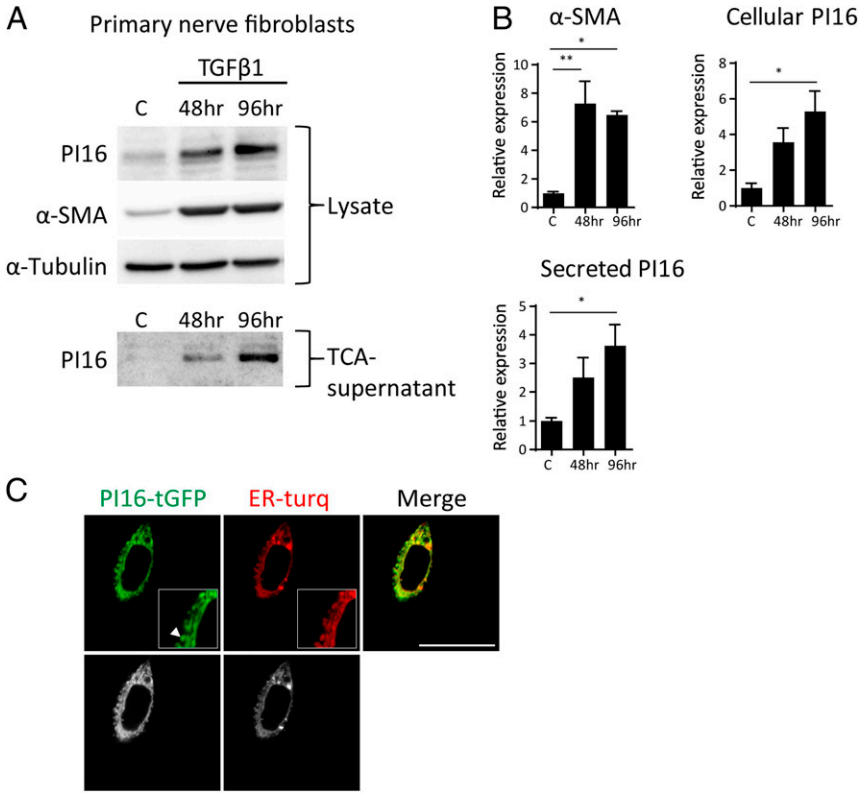

Fig. 5. Pi16 is secreted by myofibroblasts in vitro. (*A*) Mouse fibroblasts (postnatal day 8) cultured from sciatic nerve were serum starved for 24 h and treated with TGF-β1 (5 ng/mL) for 48 h or 96 h followed by Western blot analysis of total cell lysate or TCA precipitated culture supernatant. Representative Western blots are shown from three independent culture experiments. α-SMA was used as a myofibroblast marker and α-Tubulin was loading control. (*B*) Quantification of PI16 and α-SMA for *B*. Bar graph depicts means ± SEM of at least three independent experiments. $*P < 0.05$; $**P < 0.01$ (analyzed using *t* test). (*C*) Live imaging of mouse fibroblasts (L cells) transfected with mTurquoise2 (endoplasmic reticulum marker, ER-turq) and PI16 tagged with turbo-GFP (data represent images from 10 cells, three independent experiments). Raw black and white images are shown in *Lower*. Note PI16 staining in endoplasmic reticulum vesicles and tubules (arrowhead) in the magnified view in the white box. (Scale bar, 25 μm.)

endothelial barrier regulator MLC2 (*SI Appendix*, Fig. S12). Our finding that PI16, a protein that is not detectable in neurons and glia, plays a key role in neuropathic pain adds to the growing awareness that nonneuronal cell types are actively involved in chronic pain. In this respect, we see PI16 as an interesting potentially druggable target for chronic pain considering its expression is restricted to very few organs (heart, bladder, mammary, fat) (https://tabula-muris.ds.czbiohub.org/) and, crucially, genetic deletion of Pi16 does not affect cardiac function (9), although PI16 is expressed at a high level in the heart.

Until now, PI16 had not been associated with DRGs, epi/perineurium, pain, or nerve injury, and its in vivo function remained elusive. We identified Pi16 as a potential regulator of pain in an unbiased RNA screen comparing DRG samples from *Grk2*$^{+/-}$ mice who develop persistent pain and WT mice who develop transient pain in response to local inflammation in the paw. Mouse PI16 was first identified in a cardiac cDNA library and is a glycosylated protein with expression in intercellular spaces, secretory vesicles, and a predicted role in the extracellular matrix (8). PI16 is up-regulated in a mouse model of heart failure indicating a role of PI16 in cardiac hypertrophy (8, 9). However, genetic deletion of Pi16 conferred no phenotype at the level of cardiac structure or function (9). Here, we provide evidence for an in vivo function of PI16 as an important regulator of neuropathic pain. Mice with global Pi16 deletion are protected against neuropathic pain in the SNI model (Fig. 1). The protection against SNI-induced neuropathic pain in *Pi16*$^{-/-}$ mice was observed in both sexes and is not a result of gross developmental structural abnormalities in DRG or nerve (Fig. 1 and *SI Appendix*, Fig. S3). More studies are needed to determine whether the role of PI16 in pain generalizes to other models of pain, such as chemotherapy-induced neuropathic pain and inflammatory pain.

Along the pain neuroaxis, PI16 is mainly produced by fibroblasts in the meninges and in the perineurium. Consistently, mouse single-cell RNA-seq data barely detected Pi16 mRNA in 23 of 622 DRG neurons (19). We show that SNI induces expansion of predominantly α-SMA–positive fibroblasts expressing PI16 in the meninges and epi/perineurium as well as at the injury site (Figs. 2–4). Notably, SNI did not induce PI16 in neuronal, glial, and endothelial cells, or in endoneurial fibroblasts and infiltrating leukocytes in DRG and nerve. In addition, PI16 protein was not detectable in the spinal cord at baseline or after SNI. Moreover, although PI16 was detected in fibroblasts in the meninges of the spinal cord at baseline, we did not observe changes in distribution and expression upon SNI (*SI Appendix*, Fig. S6). PI16 can be secreted and, therefore, we propose it may act as a paracrine factor on anatomically closely positioned endothelial cells in the DRG (Figs. 2 and 5) and nerve. We show that SNI induces expansion of fibroblasts expressing the myofibroblast marker α-SMA in the meninges that is associated with an increase in PI16 expression as seen by Western blots and immunostaining (Figs. 3–5). It remains to be determined whether the increase in PI16 we detect in Western blots can be fully explained by the expansion of PI16^{+} cells or is also due to increased production on a per cell basis. We do know that in vitro differentiation of fibroblasts into myofibroblasts in response to TGFβ1 increased both production and secretion of PI16 (Fig. 5). Komuta et al. (20) showed TGF-β1 receptor increases in the meninges following brain injury, and

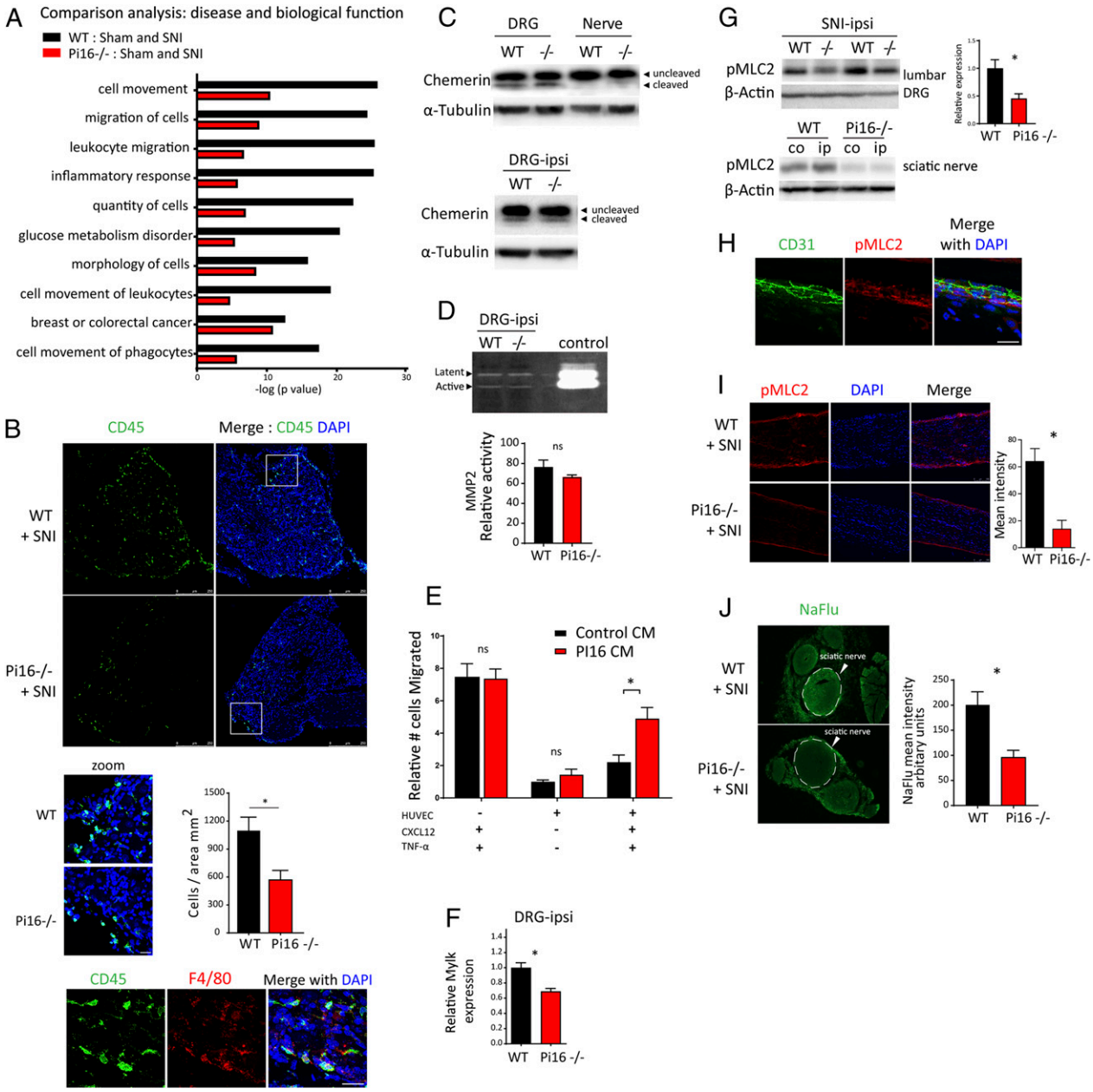

Fig. 6. Pi16 deficiency prevents the SNI-induced infiltration of leukocyte into the DRG and nerve. (*A*) IPA-based top 10 disease biological functions different in lumbar DRG from female WT and *Pi16*$^{-/-}$ mice post-SNI (day 9; $n = 3$ per group). IPA core analysis was performed between WT (WT-Sham and WT-SNI) and *Pi16*$^{-/-}$ groups (*Pi16*$^{-/-}$ Sham and *Pi16*$^{-/-}$ SNI) followed by comparison of the two core analyses. Black bars show change between WT-Sham and WT-SNI. Red bars show change between Pi16-Sham and Pi16-SNI. *y* axis denotes −log (*P* value). ($-0.5 < \log_2$ fold change < 0.5), $P < 0.05$. (*B*) Representative image of lumbar DRG ipsilateral to SNI showing immunostaining of leukocyte marker CD45 (green) and DAPI (blue) in female WT and *Pi16*$^{-/-}$ ($n = 4$) mice on SNI day 5 (*Upper*). The zoom panel shows a magnified view of the white box, and the bar graph shows quantitation data for CD45 staining from $n = 4$ mice per group. The cells were counted using Leica LAS software. *t* test: $^*P < 0.05$. (*Lower*) Shows staining of CD45 (green), macrophage marker F4/80 (red), and DAPI (blue). (*C*) Western blot analysis of chemerin protein in naïve lumbar DRG and sciatic nerve of WT and *Pi16*$^{-/-}$ male mice (*Upper*) and in DRG from ipsilateral side after SNI in WT and *Pi16*$^{-/-}$ male mice (*Lower*). (*D*) Gelatin zymography for MMP-2 activity in the lumbar DRG of SNI WT and *Pi16*$^{-/-}$ mice. Bar graph shows quantitation data from $n = 3$ male mice per group. *t* test: ns, not significant. (*E*) Effect of conditioned medium of PI16-overexpressing fibroblasts on monocyte migration across a TNF-α–activated endothelial cell monolayer in response to CXCL12 in the lower chamber either in control or PI16 conditioned medium (CM). Number of monocytes that migrated to the lower chamber are plotted; relative to those of HUVEC (+) without activation (-TNF-α) and without chemoattractant (-CXCL12), $n = 3$ samples per group; $^*P < 0.05$, two-way ANOVA, Tukey's multiple comparisons test. ns, not significant. (*F*) Real-time PCR analysis of Mylk expression in lumbar DRGs of female WT and *Pi16*$^{-/-}$ mice. $n = 3$ per group. $^{**}P < 0.01$ (analyzed using *t* test). (*G*, *Upper Left*) Western blot analysis of pMLC2 expression in ipsilateral lumbar DRGs after SNI. Blot showspMLC2 levels in two separate male WT and *Pi16*$^{-/-}$ mice, and bar graph shows quantitation data ($n = 5$ male mice per group). (*G*, *Lower Right*) Western blot analysis of pMLC2 level in sciatic nerve after SNI from contralateral (co) and ipsilateral (ip) side in WT and *Pi16*$^{-/-}$ mice. β-Actin was used as a loading control. Bar graph represents mean fluorescent intensity for pMLC2 as determined from 3 female mice per group. *t* test: $^*P < 0.05$. (*H*) Representative images showing immunostaining of pMLC2 (red), DAPI (blue), and CD31 (green) in sciatic nerve longitudinal section in WT naïve mice ($n = 3$). (*I*) Representative images showing immunostaining of pMLC2 (red) and DAPI (blue) in sciatic nerve longitudinal section from ipsilateral and contralateral side after SNI (day 5 after SNI; $n = 3$ female mice). Bar graph represents mean fluorescence intensity for pMLC2. *t* test: $^*P < 0.05$. (*J*) Representative fluorescent image of NaFlu extravasation in sciatic nerve cross-section. Male WT and *Pi16*$^{-/-}$ mice received 40 mg/kg NaFlu intravenously, and nerves were harvested 1 h later. Bar graph represents mean fluorescent intensity for NaFlu in the sciatic nerve (circle with dotted line) as determined from 3 mice per group. *t* test: $^*P < 0.05$. (Scale bar, 25 μm.)

TGF-β1 is involved in activating meningeal fibroblasts. Moreover, we found TGF-β1 mRNA was the primary transcriptional regulator driving changes in gene expression in response to SNI in our RNA-seq data, and this could be how PI16 is up-regulated as a result of SNI. Notably, PI16-positive fibroblasts remain restricted at the DRG borders in the meninges after SNI and did not invade the neuronal parenchyma of the DRG, making it unlikely that PI16 directly targets nociceptors. Collectively, our data indicate that meningeal fibroblasts are the main source of the PI16 that regulates SNI-induced pain. However, PI16 is expressed in mesenchymal stem cells in muscle and in some other tissues including heart, bladder, gat, and mammary gland (https://tabula-muris.ds.czbiohub.org/). Therefore, we cannot fully exclude a contribution of PI16 produced by other cells or tissues to pain.

A combination of transcriptomic, immunofluorescence, and cell culture studies employed here revealed that PI16 promotes migration of immune cells across the endothelial barrier. In vivo, deficiency of *Pi16* caused reduced infiltration of leukocytes in DRG as tested on day 5 after SNI (Fig. 6) and $Pi16^{-/-}$ mice were protected against SNI-induced pain (Fig. 1). Conversely, in vitro PI16-conditioned medium promotes migration of immune cells in a transendothelial migration assay (Fig. 6). RNA-seq analysis of lumbar DRGs from SNI-treated mice revealed multiple cellular infiltration and migration pathways were down-regulated in $Pi16^{-/-}$ mice (Fig. 6). Genes involved in these functional networks were mostly cytokines (e.g., *Crh*, *Csf1*, *Cxcl4*, *Ccl9*, *Timp1*, *Il1rn*, *Ccl2*, *Spp1*, *Il6*); growth factors (e.g., *Fgf3*, *Grp*, *Igf1*, *Angpt1*, *Nog*); GPCRs (*Mc4r*, *Gpr34*, *Cysltr1*, *Ccr5*, *Ccr2*, *Ccr1*, *Cx3cr1*, *C3ar1*); extracellular proteins (e.g., *serpine1*, *Lgals3*, *Tnc*, *Coch*, *Lgalgs1*, *Olfm4*, *Igfbp3*, *Cfh*); signaling kinases (e.g., *Camk1*, *Pik3cg*, *Mylk*, *Cdkn1a*, *Egfr*, *Csfr1*, *Ddr2*, *Tgfbr1*); and transmembrane receptors (e.g., *Tnfrsf8*, *Msr1*, *Fcer1g*, *Tlr7*, *Plaur*, *Il17ra*, *Il1r1*, *Cd72*, *Lilrb3*, *Cr2*, *Trem2*, *Igam*, *Cxadr*, *Unc5b*). A representation of genes from different protein families reflects a multilevel impact of reduced cellular infiltration caused by Pi16 deficiency. It remains to be determined which of these occur downstream of changes in leukocyte infiltration in $Pi16^{-/-}$ mice.

How does PI16 influence the migration of leukocytes into the DRG? PI16-dependent regulation of chemerin and MMP2 has been proposed, and these proteins can regulate leukocyte migration and infiltration (9, 11). However, we did not detect changes in the level of processed chemerin or MMP2 when comparing samples from WT and $Pi16^{-/-}$ mice under naïve conditions or after SNI (Fig. 6). An increase in the permeability of the blood–nerve barrier following nerve injury has been shown to drive neuropathic pain by facilitating extravasation of immune cells into the nerve (21). Our RNA-seq data following SNI indicated an interaction between PI16 and the kinase MLCK. MLCK and its substrate MLC2 maintain integrity of endothelial barrier, and their function has been highlighted in diseased models of lung injury, pancreatitis, and atherosclerosis (18, 22–25). In response to SNI, $Pi16^{-/-}$ mice have reduced Mlck expression and lower levels of phospho-MLC2 in DRG and sciatic nerve and reduced cellular infiltration as well as vascular permeability as measured using sodium fluorescence levels in the nerve. The specific mechanism how PI16 modulates the MLCK/MLC-2 pathway in endothelial cells remains to be established.

Taken together, our findings support a model in which nerve injury enhances production of PI16 by meningeal and epi/perineurial fibroblasts, which promotes SNI-induced neuropathic pain by increasing the permeability of the endothelial barrier and facilitating immune cell infiltration into DRG and nerve (*SI Appendix*, Fig. S12). We also propose that PI16-mediated control of MLCK-dependent phosphorylation of MLC-2 contributes to the increased permeability of the endothelial barrier in neuropathic pain. In view of the limited cellular and organ distribution of PI16, we propose that PI16 represents an attractive potential target for pain management that is unlikely to have abuse liability.

Materials and Methods

Animals. We used male and female B6:129S mice homozygous for global Pi16 deletion (Modified Medical Research Council (MMRC) stock no. 032520-UCD) and their WT control littermates at an age of 8–12 wk. All procedures followed the ARRIVE (Animal Research: Reporting of In Vivo Experiments) guidelines and are in accordance with NIH *Guidelines for the Care and Use of Laboratory Animals* (26) and the Ethical Issues of the International Association for the Study of Pain (27). Assays were performed by investigators blinded to treatment. SNI surgery was performed as described previously (28, 29). Mechanical allodynia was measured as the hind paw withdrawal response to von Frey hair stimulation (30).

Cell Culture and Reagents. Mouse perineurial fibroblasts (M1710-57, ScienCell Research Laboratories) were cultured in complete fibroblast medium (ScienCell Research Laboratories catalog no. 2301) per the manufacturer's instructions and treated with 5 ng/mL TGF-β1 (7666-MB, R&D Systems) for differentiation of fibroblasts to myofibroblasts. Human umbilical vein endothelial cells (HUVEC) cells (PromoCell C-12203) were cultured in Endothelial Cell Growth medium (PromoCell C-22210) supplemented with Supplmix (C-39215). L cells (American Type Culture Collection CRL-2648) were cultured in high glucose Dulbecco's modified Eagle medium (GE Healthcare) plus 10% fetal bovine serum (Gibco).

RNA Extraction, Library Preparation for Sequencing, and RNA-Seq Data Analyses. Transcriptional changes in the lumbar DRGs were investigated using whole-genome RNA sequencing by the RNA Sequencing Core Lab at MD Anderson Cancer Center. RNA-seq was performed on triplicate samples, and the RNA integrity number for all samples was >7. The sample libraries were generated using the Stranded mRNA-Seq kit (Kapa Biosystems) following the manufacturer's guidelines. A 75-nt paired-end run format was performed using a HiSeq 4000 Sequencer as previously described (31).

Immunofluorescence and Microscopy. Tissues were collected from mice perfused with phosphate buffered saline (PBS) followed by 4% paraformaldehyde (PFA). Spinal cord meninges were gently peeled with forceps from the vertebrae in a single layer. Sections were stained with: PI16 (1:75, R&D Systems AF4929), GLUT1 (1:250, Abcam ab652), α-SMA (1:100, Abcam ab5694), P4HB (1:250, Abcam ab137110), IBA1 (1:300, Wako 019-19741), NFH (1:200, Millipore AB1989), CGRP (1:200, Abcam ab36001), IB4 (1:100, Vector Labs B-1205), CD31 (1:50, Abcam Ab28364), CLDN1 (1:250, Abcam ab15098), Collagen IV (1:100, Southern Biotech 1340-01), PGP9.5 (1:500, Abcam ab108986), P4HB (Abcam ab137110), CD45 (1:50, BD Biosciences 550539), pMLC2 (1:200, Cell Signaling 3675S). Sections were visualized using a Leica SPE DMI 4000B confocal microscope or EVOS fluorescence microscope.

Sodium Fluorescein Permeability Assay. The permeability of vascular endothelium in nerve was assayed by extravasation of the fluorescent dye sodium fluorescein (Sigma Aldrich) (21). Cross-sections of the nerve were quantified by EVOS fluorescence microscope, and the mean intensity of fluorescence and the percent area positive were calculated using NIH ImageJ software.

Transwell Assay. Transwell inserts (Corning 6.5-mm diameter insert, 5-μm pore size, PET membrane, 24-well plate) were coated with collagen I and fibronectin. HUVEC cells (2.0×10^4) were seeded in the inserts. In parallel, L cells were transfected with Pi16-tGFP and PI16 conditioned medium was prepared. On the day of assay, HUVEC cells were activated with 500 units/mL of TNFα either in control or PI16-conditioned medium following by addition of 1×10^5 THP-1 monocytes (prior treated with 300 nM phorbol 12-myristate 13-acetate (PMA) for 48 h) to the top chamber. Human CXCL12 (SDF-1α, 300–28A, 50 ng/mL) either in control or PI16-conditioned medium was added to the bottom chamber. Cells were allowed to migrate for 5 h. Inserts were washed with PBS followed by fixation with 4% PFA and staining with 0.2% crystal violet. Cells on the top of the insert were removed using a cotton swab and only cells which migrated across the membrane were counted under a microscope.

Real-Time Quantitative PCR. RT-PCR was performed using primers for Human PI16 (Hs.PT.58.39664750) and Mouse Pi16 (Mm.PT.58.8467939 and Mm.PT.58.22010817) from Integrated DNA Technologies. Deidentified human DRGs used for RT-PCR were collected from patient donors at MD Anderson Cancer Center who had provided legal written consent. The protocol was reviewed and approved by the MD Anderson Cancer Center Institutional Review Board, and the donors were undergoing spinal surgery for disease treatment wherein a spinal nerve root was sacrificed as the standard of care.

Statistics. Data are expressed as mean ± SEM. Data were analyzed using GraphPad Prism 6. Statistical analyses were carried out using *t* test (for Western blots, RT-PCR, and immunostaining data), two-way ANOVA with repeated measure followed by Bonferroni analysis (for von Frey behavior data), and two-way ANOVA followed by Tukey's analysis (for transwell migration assay). A *P* value less than 0.05 was considered significant. All animal experiments were repeated at least once with similar results. In addition, at least two independent technical replicates were performed for IHC where different sections of the same tissue were stained and observed/imaged to check for consistency. We performed biochemical analysis (Western blots, IHC) in mixed groups of males and females unless specified otherwise in the legend. We did not detect major differences but were not powered to fully assess potential sex differences in magnitudes of effects.

Data Availability. RNA-seq data reported in this paper have been deposited in Zenodo repository (https://zenodo.org/record/3473295). *Pi16*$^{-/-}$ mice embryos are available at MMRC (stock no. 032520-UCD). A detailed description of methods is provided in *SI Appendix*. Access to additional raw data and protocols used in this work can be requested by contacting the corresponding author.

ACKNOWLEDGMENTS. This work was supported by National Institute of Neurological Disorders and Stroke of the NIH Grants R01 NS073939 and R01 NS074999. We thank Kenneth Dunner Jr. at the High Resolution Electron Microscopy Facility at MD Anderson Cancer Center for tissue processing and image capturing and Ms. Itee Mahant, Dr. Angie C.A. Chiang, Ms. Jenolyn Alexander, and Mr. Jules D. Edralin for technical help.

1. L. S. Simon, Relieving pain in America: A blueprint for transforming prevention, care, education, and research. *J. Pain Palliat. Care Pharmacother.* **26**, 197–198 (2012).
2. D. J. Gaskin, P. Richard, The economic costs of pain in the United States. *J. Pain: Official J. Am. Pain Soc.* **13**, 715–724 (2012).
3. N. Eijkelkamp *et al*., Low nociceptor GRK2 prolongs prostaglandin E2 hyperalgesia via biased cAMP signaling to Epac/Rap1, protein kinase Cepsilon, and MEK/ERK. *J. Neurosci.* **30**, 12806–12815 (2010).
4. P. Singhmar *et al*., Critical role for Epac1 in inflammatory pain controlled by GRK2-mediated phosphorylation of Epac1. *Proc. Natl. Acad. Sci. U.S.A.* **113**, 3036–3041 (2016).
5. H. Wang *et al*., Balancing GRK2 and EPAC1 levels prevents and relieves chronic pain. *J. Clin. Invest.* **123**, 5023–5034 (2013).
6. N. Eijkelkamp *et al*., GRK2: A novel cell-specific regulator of severity and duration of inflammatory pain. *J. Neurosci.* **30**, 2138–2149 (2010).
7. G. M. Gibbs, K. Roelants, M. K. O'Bryan, The CAP superfamily: Cysteine-rich secretory proteins, antigen 5, and pathogenesis-related 1 proteins–roles in reproduction, cancer, and immune defense. *Endocr. Rev.* **29**, 865–897 (2008).
8. R. J. Frost, S. Engelhardt, A secretion trap screen in yeast identifies protease inhibitor 16 as a novel antihypertrophic protein secreted from the heart. *Circulation* **116**, 1768–1775 (2007).
9. M. Regn *et al*., Peptidase inhibitor 16 is a membrane-tethered regulator of chemerin processing in the myocardium. *J. Mol. Cell. Cardiol.* **99**, 57–64 (2016).
10. N. Lupsa *et al*., Skin-homing CD8(+) T cells preferentially express GPI-anchored peptidase inhibitor 16, an inhibitor of cathepsin K. *Eur. J. Immunol.* **48**, 1944–1957 (2018).
11. G. G. Hazell *et al*., PI16 is a shear stress and inflammation-regulated inhibitor of MMP2. *Sci. Rep.* **6**, 39553 (2016).
12. R. S. Tubbs *et al*., Meningeal relationships to the spinal nerves and rootlets: A gross, histological, and radiological study with application to intradural extramedullary spinal tumors. *Childs Nerv. Syst.* **31**, 675–681 (2015).
13. C. Stolinski, Structure and composition of the outer connective tissue sheaths of peripheral nerve. *J. Anat.* **186**, 123–130 (1995).
14. I. C. Nicholson *et al*., PI16 is expressed by a subset of human memory Treg with enhanced migration to CCL17 and CCL20. *Cell. Immunol.* **275**, 12–18 (2012).
15. U. Ozerdem, K. A. Grako, K. Dahlin-Huppe, E. Monosov, W. B. Stallcup, NG2 proteoglycan is expressed exclusively by mural cells during vascular morphogenesis. *Dev. Dyn.* **222**, 218–227 (2001).
16. L. Richard, N. Védrenne, J. M. Vallat, B. Funalot, Characterization of endoneurial fibroblast-like cells from human and rat peripheral nerves. *J. Histochem. Cytochem.* **62**, 424–435 (2014).
17. J. R. Perkins *et al*., A comparison of RNA-seq and exon arrays for whole genome transcription profiling of the L5 spinal nerve transection model of neuropathic pain in the rat. *Mol. Pain* **10**, 7 (2014).
18. R. R. Rigor, Q. Shen, C. D. Pivetti, M. H. Wu, S. Y. Yuan, Myosin light chain kinase signaling in endothelial barrier dysfunction. *Med. Res. Rev.* **33**, 911–933 (2013).
19. D. Usoskin *et al*., Unbiased classification of sensory neuron types by large-scale single-cell RNA sequencing. *Nat. Neurosci.* **18**, 145–153 (2015).
20. Y. Komuta *et al*., Expression of transforming growth factor-β receptors in meningeal fibroblasts of the injured mouse brain. *Cell. Mol. Neurobiol.* **30**, 101–111 (2010).
21. T. K. Lim *et al*., Blood-nerve barrier dysfunction contributes to the generation of neuropathic pain and allows targeting of injured nerves for pain relief. *Pain* **155**, 954–967 (2014).
22. S. Recoquillon *et al*., Non-muscular myosin light chain kinase triggers intermittent hypoxia-induced interleukin-6 release, endothelial dysfunction and permeability. *Sci. Rep.* **7**, 13664 (2017).
23. Z. M. Goeckeler, R. B. Wysolmerski, Myosin light chain kinase-regulated endothelial cell contraction: The relationship between isometric tension, actin polymerization, and myosin phosphorylation. *J. Cell Biol.* **130**, 613–627 (1995).
24. Y. Xiong *et al*., Myosin light chain kinase: A potential target for treatment of inflammatory diseases. *Front. Pharmacol.* **8**, 292 (2017).
25. M. S. Wainwright *et al*., Protein kinase involved in lung injury susceptibility: Evidence from enzyme isoform genetic knockout and in vivo inhibitor treatment. *Proc. Natl. Acad. Sci. U.S.A.* **100**, 6233–6238 (2003).
26. National Research Council, *Guide for the Care and Use of Laboratory Animals* (National Academies Press, Washington, DC, ed. 8, 2011).
27. M. Zimmermann, Ethical guidelines for investigations of experimental pain in conscious animals. *Pain* **16**, 109–110 (1983).
28. I. Decosterd, C. J. Woolf, Spared nerve injury: An animal model of persistent peripheral neuropathic pain. *Pain* **87**, 149–158 (2000).
29. G. Laumet *et al*., Upregulation of neuronal kynurenine 3-monooxygenase mediates depression-like behavior in a mouse model of neuropathic pain. *Brain Behav. Immun.* **66**, 94–102 (2017).
30. S. R. Chaplan, F. W. Bach, J. W. Pogrel, J. M. Chung, T. L. Yaksh, Quantitative assessment of tactile allodynia in the rat paw. *J. Neurosci. Methods* **53**, 55–63 (1994).
31. G. S. Chiu *et al*., Nasal administration of mesenchymal stem cells restores cisplatin-induced cognitive impairment and brain damage in mice. *Oncotarget* **9**, 35581–35597 (2018).